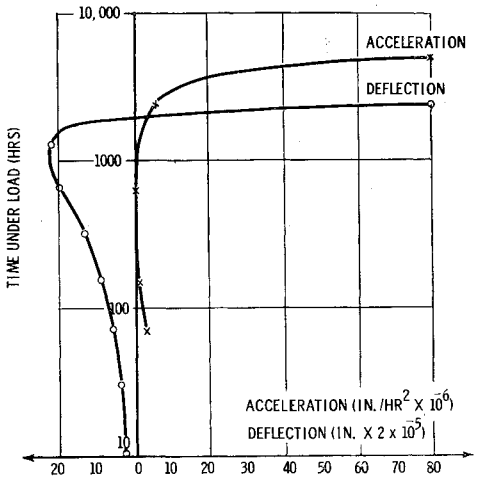

Fig. 3 Vertical deflection and acceleration vs time for a point located at 14/32 L distance from the edge.

stress level, the amount of existing creep strain, the temperature, and the duration of the time increment that the stress level remains constant.

Due to the incremental nature of the procedure, the strain at the end of ith increment is represented as

$$\epsilon'' = C_i t_i^{k_i} \text{ where } C_i = A_i \sinh B\sigma_i \text{ and } t_i = t_{i-1}{}^* + \Delta t_i \quad (6)$$

Using a recurrence relationship, each $t_i{}^*$ also is represented in terms of the previous ones:

$$t_i{}^* = C_1{}^{1/k_{i+1}} C_{i+1}{}^{-1/k_{i+1}} (t_{i-1}{}^* + \Delta t_i{}^*)^{k_i/k_{i+1}} \quad (7)$$

which, in turn, leads to the elimination of the t^* from Eq. (6). In the example problem, temperature remains constant during the life of the structure, and time increments are taken such that the logarithmic time increment goes to a constant value as i increases. Then the resulting creep strain is

$$\epsilon_i'' = \left(\Delta t \sum_i C_i{}^{1/k} \rho^{i-1}\right)^k \text{ where } \rho = \Delta t_{i+1}/\Delta t_i \quad (8)$$

Discussion of Results

The behavior of the integrally stiffened panel as idealized in this study suggested two interesting points: 1) the possibility of determining the time-dependent deflection pattern of either a stiffened panel or a panel with intermediate supports by a simple numerical procedure, and 2) the possibility of establishing a safe allowable creep life for compression instability. As indicated in Ref. 4, the existing creep buckling data suggest a relation between the $w_{,tt}$ and the allowable compression life of a column. In Ref. 5, Gerard suggested the $w_{m,\,t}/w_m = 0$, following an infinitesimal lateral disturbance applied to a perfect column, as the stability criterion for creep buckling. In the case of initial imperfectness, there is no need for the infinitesimal lateral disturbance for the purpose of inspection and, if the time of $w_{m,\,tt} = 0$ is taken as the limit of the useful life, the column is considered safe to carry the load as long as it keeps deflecting at a decreasing rate.

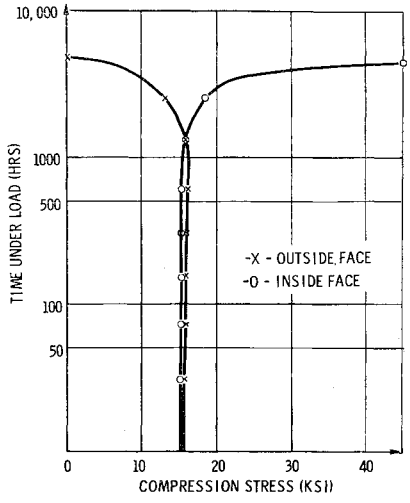

Fig. 4 Stress on panel faces vs time at a point located at 14/32 L distance from the edge.

Figures 2 and 3 demonstrate the time-dependent deflection pattern, and the relation between the time of zero deceleration and the time required to reach the stage of unbound deflection. In Fig. 4, the relation between the stress levels on the concave and the convex surfaces and the time under compressive load has been shown. This can be explained by observing that the material on the concave side of the panel is under the influence of two factors. The first one is the amount of creep strain, and, due to the strain hardening, creep rate reduces as the creep strain increases. The second factor is the acting stress that increases as the curvature increases, thus increasing the creep rate. During the time period immediately following the application of the load, the influence of the strain hardening is more pronounced and it causes the panel to deflect at a decreasing rate. At time $w_{m,\,tt} = 0$, the influence of these two factors balance each other, and from then on, the panel deflects at an ever increasing rate and finally collapses. Therefore, it can be concluded that the time of zero deceleration could have been taken as the safe allowable time for the compression life of the panel.

Appendix A

The numerical results shown in Figs. 2 and 3 are obtained with the following values of constants: $L = 24.00$ in.; $a = 0.0123$ in.; $h = 0.1230$; support height = 1.0 in.; support width = 0.25 in.; $E = 9.4 \times 10^6$ psi; $\mu = 0.3$; $A = 6.8 \times 10^{-5}$; $B = 9300^{-1}$ psi; $k = 0.5$; applied compressive load = 1900 lb/in. The material is 2024-T3 aluminum alloy at 400°F.

References

[1] Lin, T. H., "Creep stresses and deflections of columns," J. Appl. Mech. **23**, 214–219 (1956).

[2] Kennedy, A. J., *Processes of Creep and Fatigue in Metals* (John Wiley & Sons Inc., New York, 1963), p. 154.

[3] Dorn, J. E. and Shepard, L. A., "What we need to know about creep," Symposium on Effect of Cyclic Heating and Stressing on Metals at Elevated Temperatures, American Society for Testing Materials, Special Tech. Publ. 165 (1954).

[4] Kiciman, M., "Design study of compression creep instability," North American Aviation Inc., Rept. NA-63-699 (1963).

[5] Gerard, G. and Papirno, R., "Classical columns and creep," J. Aerospace Sci. **29**, 680–688 (1962).

Frequency and Damping from Time Histories: Maximum-Slope Method

T. Peter Neal*
Cornell Aeronautical Laboratory Inc., Buffalo, N. Y.

Introduction

DETERMINATION of the undamped natural frequency and damping ratio of highly damped second-order systems from time history data is notoriously difficult because of the lack of measurable response overshoot. The maximum-slope method is an easily-used technique developed specifically for systems having damping ratios of 0.5 to 1.4. It does not

Received October 11, 1966.

* Assistant Aeronautical Engineer, Flight Research Department.

require knowledge of the steady-state for damping ratios less than 1.0, and tends to minimize the effects of non-ideal inputs.

Description of the Method

Use of the method requires that the second-order system has its input held constant during the time between two successive peaks of the time history. (A "peak" is a point at which the time history has zero slope.) For systems having damping ratios greater than 0.5, there generally will be only two readily apparent peaks; and for damping ratios 1.0 or greater, the second peak is identically equal to the steady-state.

Straight lines having zero slope are drawn tangent to the system response X at the two peaks (see Fig. 1). Next a third tangent is drawn at a point between the peaks where the slope $\dot{X}$ is a maximum. A vertical line then is drawn through the intersection of the maximum-slope line and the tangent to the second peak. The ratio $(\Delta X_1/\Delta X)$ then is determined and used in Fig. 2 to obtain the damping ratio ζ, and the undamped natural frequency parameter $(\omega_n \Delta t)$. Next, Δt is measured and divided into $(\omega_n \Delta t)$ to obtain ω_n in radians per second.

Theoretically, any type of input can be used to excite the system. However, since the only useful portion of the response of a highly damped system is the section immediately following the input, a very sharp type of input usually is required to insure that the free response is not distorted by input transients. In practice, it often is difficult to obtain a step, pulse, or doublet input sharp enough to avoid some distortion of the response. The distortion in response shape due to such nonideal inputs usually is confined to the very early part of the response. Some methods rely on determination of the proper time to label "$t = 0$" and/or time to reach some small percentage of the steady-state. Such methods should be used with care because the results are very sensitive to even slight distortions of the initial response. The maximum-slope method avoids dependence on the initial shape. The only measurement used which involves the initial response at all is ΔX, and ΔX is relatively insensitive to input transients.

Application to Airplane Short-Period Oscillation

To illustrate the application of the maximum-slope method to systems of higher than second order, the natural frequency and damping ratio of an airplane's short-period mode will be obtained. The following equation is a generalized transfer function for a conventional airplane's longitudinal response to an elevator-stick input:

$$\frac{X(s)}{\delta_{es}(s)} = \frac{KN(s)}{[s^2 + 2\zeta_{sp}\omega_{sp} + \omega_{sp}^2]\,[s^2 + 2\zeta_p\omega_p + \omega_p^2]}$$

s $\equiv$ Laplace variable
$X(s)$ $\equiv$ generalized longitudinal response perturbation—normally angle-of-attack (α), pitch attitude (θ), flight path speed (u), or normal acceleration (n_z)
$\delta_{es}(s)$ $\equiv$ elevator-stick displacement from trim
K $\equiv$ gain (dependent on control linkages)
$N(s)$ $\equiv$ generalized numerator polynomial
ζ_{sp}, ω_{sp} $\equiv$ short-period damping ratio and undamped natural frequency, respectively
ζ_p, ω_p $\equiv$ Phugoid damping ratio and undamped natural frequency, respectively

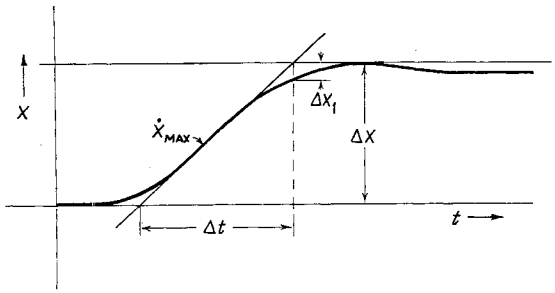

Fig. 1 Typical response of a highlydamped second-order system to a step input.

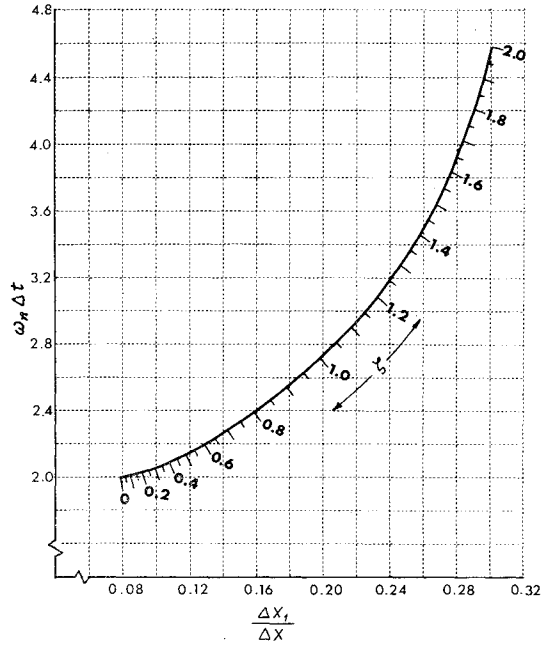

Fig. 2 Determination of ζ and $(\omega_n \Delta t)$.

The time history of any response variable X will be the sum of the two second-order oscillations. The shapes of these two component oscillations (after the input has become steady-state) do not change with the specific response variable measured or with the type of input transient used to excite the system. The shapes of the component oscillations are dependent only on ζ_{sp} ω_{sp}, ζ_p, and ω_p. The relative magnitudes and the phasing of these two components, however, are affected by numerator dynamics and the type of input, so that the total response can vary considerably with changes in these two factors.

The first step in determining ζ_{sp} and ω_{sp} is to measure the response variable that exhibits the least phugoid excitation. Such a response would normally be α. The next step is to excite the system with stick input which will emphasize the short-period mode while further suppressing the phugoid mode. A sharp doublet works very nicely for this purpose. Fig. 3 shows the α response of the USAF/CAL T-33 variable-stability airplane to an elevator-stick doublet. The phugoid mode is quite well suppressed here, but note that this input-shaping technique will work well only if ω_{sp} and ω_p are well separated [$(\omega_{sp}/\omega_p) \geqslant 4$ or 5 usually is sufficient if the measured response is α; a ratio of ten or more may be required if θ is used.]

The input of Fig. 3 essentially has reached a steady value at the α-peak at $t = 1.75$ sec. Making measurements from Fig. 3; $(\Delta X_1/\Delta X) = 0.141$, and $\Delta t = 0.49$ sec. From Fig. 2, $\zeta_{sp} = 0.68$, $(\omega_{sp}\Delta t) = 2.27$, and $\omega_{sp} = (2.27/0.49) = 4.6$ rad/sec.

Summary

The maximum-slope method is a quick and easy method for obtaining the natural frequency and damping ratio of highly damped second-order systems from time history data. The method also can be used to identify individual complex roots

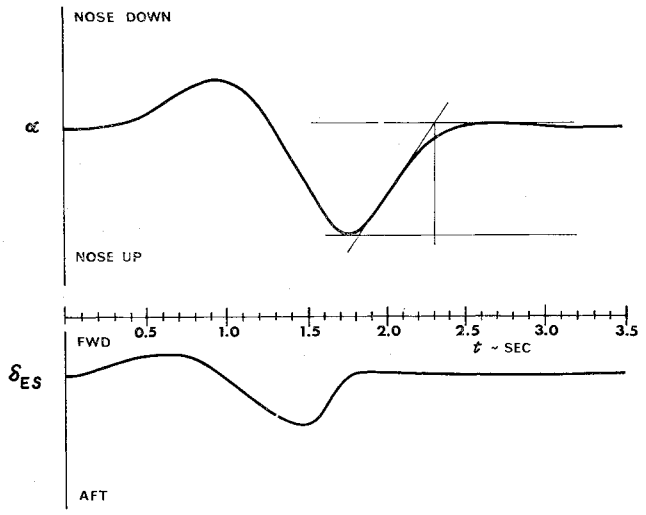

Fig. 3 Angle-of-attack response of the variable-stability T-33 to an elevator-stick doublet.

of higher-order systems when the roots are widely separated in natural frequency. The technique has particular application to identification of an airplane's short-period mode because the steady-state response need not be determined for $\zeta < 1.0$. (The steady-state response of an airplane's short-period oscillation often is masked by the presence of even small amounts of phugoid excitation).

Several other approaches to the problem of measuring airplane short-period dynamics are presented in Ref. 1, along with useful refinements of some rather well known techniques.

Reference

[1] Dolbin, B. H., "Study of some hand-computing techniques to determine the approximate short-period mode from airplane responses," Cornell Aeronautical Lab. FDM 371 (March 1966).

Supersonic and Hypersonic Lift of Highly Swept Wings and Wing-Body Combinations

A. R. ORTELL*
Hayes International Corporation, Birmingham, Ala.

Nomenclature

A = aspect ratio
c = wing root chord
c_{dc} = cross-flow drag coefficient
C_N = normal-force coefficient
$C_{N\alpha}$ = rate of change of normal-force coefficient with angle of attack
$K_{W(B)}$ = lift ratio, wing in presence of body
$K_{B(W)}$ = lift ratio, body in presence of wing
M = Mach number
S_{nose} = maximum cross-sectional area of body nose
S_{plan} = planform area
S_{ref} = reference area
S_{wexp} = exposed area of wing
t = wing thickness at root
α = angle of attack
β = $(M^2 - 1)^{1/2}$
ϵ = wing semi-apex angle
λ = wing taper ratio

Received August 18, 1966.
* Manager, Weapons Research.

VARIOUS inviscid flow methods have been applied to the problem of predicting the nonlinear lift component of highly swept low aspect ratio wings as a function of angle of attack and Mach number. Such methods in their complete form are generally too unwieldy for preliminary design purposes and, when simplified, tend to be unacceptably inaccurate.

The nonlinearity in the lift of low aspect ratio swept wings is due to a characteristic viscous cross flow that is manifested as a strong vortical type of flow separation along the leading edge. This flow separation is not unlike that occurring along an inclined slender body of revolution, and it is this fact that is utilized in the method described in this note.

In Ref. 1, it is shown that the lift on an inclined cylinder due to viscous cross flow can be expressed approximately as

$$C_{N\text{vis}} = c_{d_c} (S_{\text{plan}}/S_{\text{ref}}) \sin^2\alpha \quad (1)$$

where c_{d_c} is the drag coefficient experienced by a two-dimensional circular cylinder at a Mach number based on the cross component of velocity ($M \sin\alpha$). The variation of c_{d_c} with cross-flow Mach number is illustrated in Fig. 1.

The total lift for a low aspect ratio wing can then be considered to be the sum of the usual linear nonviscous term and the viscous cross flow term, thus:

$$C_{NT} = (C_{N_\alpha})\alpha + c_{d_c} (S_{\text{plan}}/S_{\text{ref}}) \sin^2\alpha \quad (2)$$

In the case of symmetrical wing-body combinations it is necessary to introduce the slender-body nose lift term and wing-body interference lift factors of Ref. 2. For a wing-body combination the lift equation becomes

$$C_{NT} = [K_{W(B)} + K_{B(W)}](C_{N_\alpha})\alpha \frac{S_{\text{wexp}}}{S_{\text{ref}}} + 2\alpha \frac{S_{\text{nose}}}{S_{\text{ref}}} + c_{d_c} \frac{S_{\text{plan}}}{S_{\text{ref}}} \sin^2\alpha \quad (3)$$

The planform area in the viscous lift term of Eq. (3) is the combined area of wings and body.

Equations (2) and (3) have been applied to a large number of wing-alone and wing-body configurations, and the results have been compared with wind-tunnel data. Only delta and clipped-delta wings with unswept trailing edges were considered. Although Eqs. (2) and (3) produced the proper trends, it was necessary to further correlate predicted lift values with experimental data in terms of wing semi-apex angle, angle of attack, and Mach number to obtain acceptable accuracy. This correlation is presented in Fig. 2 in the form of a correction factor to be applied to the calculated lift values. The correlating parameter $\beta \tan\epsilon$ is the usual supersonic linear theory similarity parameter; however, the other

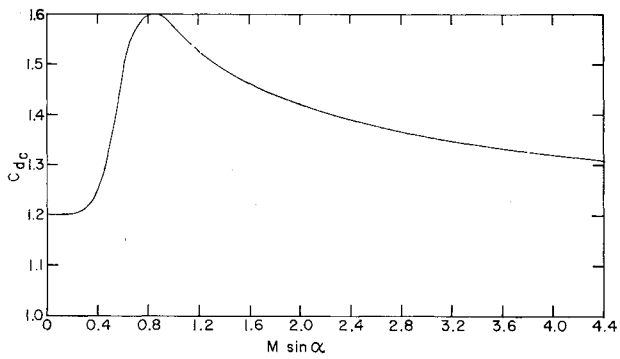

Fig. 1 Circular cylinder drag coefficient for viscous cross-flow calculations.